Journal of Medicinal Chemistry

pubs.acs.org/jmc

Article

Design of Thioether Cyclic Peptide Scaffolds with Passive Permeability and Oral Exposure

Andrei A. Golosov,[#] Alec N. Flyer,[#] Jakal Amin, Charles Babu, Christian Gampe, Jingzhou Li, Eugene Liu, Katsumasa Nakajima, David Nettleton, Tajesh J. Patel, Patrick C. Reid, Lihua Yang, and Lauren G. Monovich*[,#]

Cite This: *J. Med. Chem.* 2021, 64, 2622−2633

Read Online

ACCESS | Metrics & More | Article Recommendations | Supporting Information

ABSTRACT: Advances in the design of permeable peptides and in the synthesis of large arrays of macrocyclic peptides with diverse amino acids have evolved on parallel but independent tracks. Less precedent combines their respective attributes, thereby limiting the potential to identify permeable peptide ligands for key targets. Herein, we present novel 6-, 7-, and 8-mer cyclic peptides (MW 774−1076 g·mol^{-1}) with passive permeability and oral exposure that feature the amino acids and thioether ring-closing common to large array formats, including DNA- and RNA-templated synthesis. Each oral peptide herein, selected from virtual libraries of partially N-methylated peptides using *in silico* methods, reflects the subset consistent with low energy conformations, low desolvation penalties, and passive permeability. We envision that, by retaining the backbone N-methylation pattern and consequent bias toward permeability, one can generate large peptide arrays with sufficient side chain diversity to identify permeability-biased ligands to a variety of protein targets.

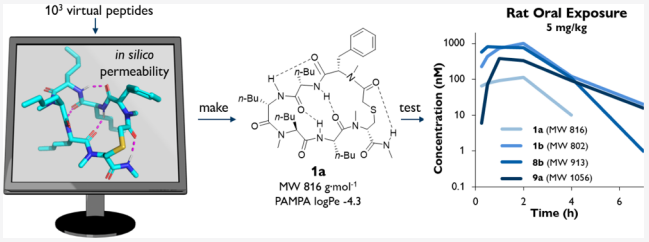

INTRODUCTION

Interest in cyclic peptides as therapeutics[1,2] is renewed by a growing awareness of design principles governing their passive cellular permeability[3−6] and by exponential advances in the construction and screening of cyclic peptide libraries, especially those including noncanonical amino acids.[7−9] However, published cases wherein cyclic peptides combine passive permeability and oral bioavailability with high affinity for a target protein are dominated by natural products.[10−15] The present contribution provides an approach to identify permeable peptide ligands to therapeutic targets. Traditionally, permeable macrocyclic peptides are identified by discrete synthesis and careful side chain variation of privileged, natural product scaffolds.[16−21] Macrocyclic peptides with passive permeability sample conformations with low desolvation penalties upon transfer from aqueous to membrane environments.[4,22] More recently, the basic principles governing passive permeability were applied to the prospective design of macrocyclic peptides with oral exposure.[23,24] However, the limited diversity of permeable macrocyclic peptide scaffolds presents a challenge for their identification as protein ligands. By contrast, cell-free, *in vitro* translation of peptides on modified ribosomes offers enormous, highly diverse libraries of macrocyclic peptides containing both canonical and noncanonical amino acids and entry to macrocyclic peptide ligands with exquisite affinity and selectivity.[25−28] However, in this context, ligands are discovered in the absence of selection pressure for cellular permeability.

Consistent with the hypothesis that permeability is a limiting factor for the oral exposure of cyclic peptides, we present 6-, 7-, and 8-mer thioether macrocyclic peptides that are both permeable and orally exposed. Starting from a virtual library of macrocycles with varied, partial backbone N-methylation, each example macrocycle herein was selected for permeability using *in silico* methods and then synthesized and validated by *in vitro* and/or *in vivo* experiment. The specific N-methylation sites within each macrocyclic peptide govern conformation and intramolecular hydrogen-bond network and also bias them for permeability. Therefore, each case described herein is a foundational member of a family of analogues that share the same macrocycle backbone, N-methylation pattern, and permeability bias. We show herein, through a brief survey of lipophilic side chain analogues with shared backbone and N-methylation sites, that the permeability and oral exposure of the parent example can be ported to its family members. More broadly, we chose the specific amino acids and thioether ring-closing to be compatible with a variety of library technologies, including synthesis and screening by *in vitro* translation

Received: August 28, 2020
Published: February 25, 2021

https://dx.doi.org/10.1021/acs.jmedchem.0c01505
J. Med. Chem. 2021, 64, 2622−2633

platforms, to better enable the identification of permeable ligands to therapeutic targets.

RESULTS AND DISCUSSION

In Silico Optimization of the N-Methylation Pattern. By analogy to published work on the *de novo* discovery of passive cell membrane permeable peptides,[29] we selected 6-mer macrocycles to begin our investigations. Similar to prior efforts, we hypothesized that an optimal N-methylation pattern for permeability could stabilize a macrocyclic conformation with a low desolvation penalty for transit from an aqueous to membrane environment. However, we substituted the empirical on-resin N-methylation described previously with an *in silico* analysis of virtual compound libraries; this also removes the conformational biases of the unmethylated on-resin parent peptide. The subset of virtual compounds with N-methylation patterns predicted to have low desolvation penalty and, therefore, enhanced permeability (plus comparator control compounds) was selected for chemical synthesis.

A common ring-closing strategy for macrocyclic peptides generated by *in vitro* translation features the reaction of a C-terminal cysteine onto an N-terminal electrophilic capping group to yield a cysteine thioether.[30] No examples of orally bioavailable, thioether-containing macrocycles have been described to date, so we decided to investigate a thioether ring-closing strategy by analogy to those commonly used with *in vitro* translated peptides.

The cysteine (Cys) used to effect the macrocyclic ring closure was held constant as the C-terminal residue and capped as a methyl amide, which we chose in order to limit the number of H-bond donors at the C-terminus to one (Chart 1).

Chart 1. Workflow for Identification of Permeable 6-mer Macrocycles[a]

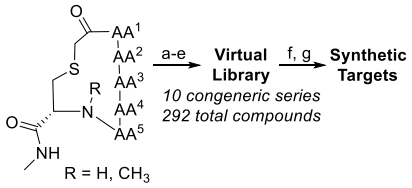

[a]Workflow steps: (a) select amino acid residue AA^1 from Phe, Phe, phe, or phe; (b) select amino acid residues AA^{2-5} from Nle, Nle, or Pro; (c) exclude cases with more than one Pro; (d) allow R = H or CH_3; (e) exclude combinations with more than 3 N-methylations; (f) sample conformations for all virtual library members; and (g) triage based on $\Delta G^*_{transfer}$ and conformational analysis.

We evaluated virtual compounds with both unmethylated and backbone N-methylated Cys *in silico*, although *N*-methyl Cys may not be optimal for *in vitro* translation systems. To provide a UV chromophore, the N-terminal amino acid AA^1 was selected from phenylalanine variants, including either enantiomer of phenylalanine (Phe or D-Phe (phe)) or N-methylated L- or D-phenylalanine (Phe or phe). Residues AA^{2-5} were selected from Pro, norleucine (Nle), or norleucine with backbone methylation (Nle). Norleucine, with and without backbone methylation, was chosen as a model hydrophobic residue for its compatibility with specialized *in vitro* translation methods and structural similarity to the Leu residues in oral natural products [*e.g.*, cyclosporine A (CsA)] and oral peptides (*e.g.*, 1NMe3). We allowed up to one proline (Pro) and, for synthetic ease on bead or *in vitro*, no more than three total residues with N-methylation.

The unique conformational bias introduced by proline segregated its four unique positions along the chain (AA^{2-5}), plus proline null, into five separate congeneric series. The phenylalanine stereochemistry (L- or D-) bifurcated each of the five proline series, to produce a total of 2 × 5, or 10, congeneric series. For example, Series A and Series B feature L- or D-phenylalanine, respectively, in the absence of proline at AA^{2-5}. *In silico* selections were performed within each congeneric series. Computational models of all possible N-methylated variants with 0−3 N-methylated residues were generated for each of the ten congeneric series. Conformations of the resulting 292 virtual peptides were sampled in low dielectric medium as a model of the nonpolar portion of the membrane. The transfer free energy from water to membrane was computed as $\Delta G_{transfer}$ for each conformation.[31] Thereafter, we performed an analysis of conformations with the lowest energy and the lowest $\Delta G_{transfer}$ values for each virtual compound. The term $\Delta G^*_{transfer}$ reflects the transfer free energy calculation combined with conformational analysis. We anticipated $\Delta G^*_{transfer}$ to be useful for identifying compounds with low $\Delta G_{transfer}$ values and conformations with the fewest solvent-exposed backbone NHs. We considered both $\Delta G_{transfer}$ and $\Delta G^*_{transfer}$ values during the selection of compounds for synthesis to evaluate the utility of each to select for permeable macrocycles.

Synthesis. Synthesis of reference 6-mers, plus a subset of N-methylated 6-mer comparators selected *in silico*, was conducted on resin using an automated peptide synthesizer (Scheme 1). The C-terminal-protected cysteine was coupled to

Scheme 1. General Synthetic Route for 6-mer Macrocycles[a]

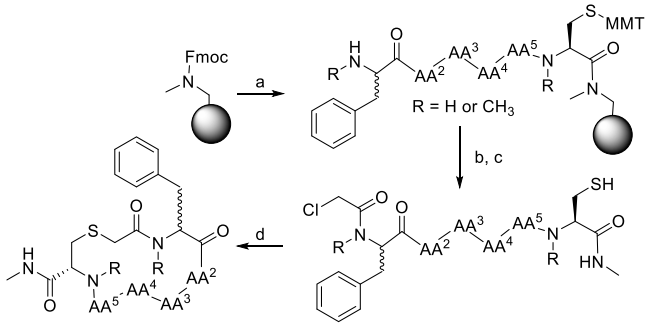

[a]Reagents and conditions: (a) automated peptide synthesis (details in experimental); (b) 5 equiv 2,5-dioxopyrrolidin-1-yl-2-chloroacetate, NMP, 23 °C; (c) TFA/H_2O/TIS 92.5:2.5:5; and (d) Et_3N, DMSO, 23 °C, 5−15% yield (over 4 steps).

the resin, followed by the series of five variable residues. The first four variable residues were chosen from norleucine (Nle), *N*-methylnorleucine (Nle), or proline (Pro). The *N*-terminal residue, selected from phenylalanine (Phe), D-phenylalane (phe), *N*-methylphenylalanine (Phe), or *N*-methyl-D-phenylalanine (phe), was capped with a chloroacetyl electrophile. Subsequent deprotection of the cysteine and release from the resin, followed by ring-closing nucleophilic attack of the cysteine side chain onto the chloroacetyl moiety, afforded the desired macrocyclic thioethers, representing Series A−J.

Measured Properties. Data for representative compounds from congeneric Series A−G are presented as Table 1. Series H−J did not produce N-methylated structures with promising

https://dx.doi.org/10.1021/acs.jmedchem.0c01505
J. Med. Chem. 2021, 64, 2622−2633

Table 1. Calculated and Measured Property Data for Congeneric Series A−G

series	Cmpd	AA[1]	AA[2]	AA[3]	AA[4]	AA[5]	R	$\Delta G^*_{transfer}$ (kcal·mol^{-1})	exposed NHs (count)	PAMPA log P_{app}
A	**1**	Phe[a]	Nle[d]	Nle	Nle	Nle	H	−4.30	3	<−5.9
	1a	Phe	Nle	Nle	Nle	Nle	CH_3	−6.25	0	−4.3
	1b	Phe	Nle	Nle	Nle	Nle	H	−5.44	0	−4.3
B	**2**	phe[b]	Nle	Nle	Nle	Nle	H	−4.45	2	<−6.0
	2a	phe	Nle[e]	Nle	Nle	Nle	H	−7.55	0	−4.6
	2b	phe	Nle	Nle	Nle	Nle	H	−5.78	1	−5.1
	2c	phe	Nle	Nle	Nle	Nle	H	−4.26	1	−5.1
	2d	phe	Nle	Nle	Nle	Nle	CH_3	−2.65	2	<−6.0
	2e	phe	Nle	Nle	Nle	Nle	H	−5.16	3	<−5.7
C	**3**	Phe	Nle	Nle	Nle	Pro[f]	H	−2.24	4	<−6.7
	3a	Phe[c]	Nle	Nle	Nle	Pro	H	−3.41	0	−5.5
D	**4**	phe	Nle	Nle	Nle	Pro	H	−2.29	3	<−6.7
	4a	phe	Nle	Nle	Nle	Pro	H	−3.23	0	<−5.6
E	**5**	Phe	Nle	Nle	Pro	Nle	H	−0.27	4	−5.9
	5a	Phe	Nle	Nle	Pro	Nle	H	−3.22	0	−4.5
F	**6**	phe	Nle	Nle	Pro	Nle	H	−0.63	2	−5.8
	6a	phe	Nle	Nle	Pro	Nle	H	−2.03	0	−4.6
G	**7**	Phe	Nle	Pro	Nle	Nle	H	3.69	4	−5.8
	7a	Phe	Nle	Pro	Nle	Nle	CH_3	−3.56	0	−4.5

[a]Phe (phenylalanine). [b]phe (D-phenylalanine). [c]Phe (*N*-Me-phenylalanine). [d]Nle (norleucine). [e]Nle (*N*-Me-norleucine). [f]Pro (proline).

$\Delta G^*_{transfer}$ values and so were not prepared. For the parent compound **1** of congeneric Series A (AA[1] = Phe, AA[2−5] = Nle), the calculated −4.30 kcal·mol^{-1} $\Delta G^*_{transfer}$ is associated with three exposed backbone NHs and undetectable permeability in the PAMPA assay (log P_{app} < −5.9). Judicious addition of two backbone methylations in either compound **1a** (AA[4] and Cys) or **1b** (AA[3] and AA[5]) lowered $\Delta G^*_{transfer}$ by 1.95 or 1.14 kcal·mol^{-1}, respectively, and eliminated solvent-exposed backbone NHs. Accordingly, the PAMPA data for **1a** and **1b** (log P_{app} −4.3 and −4.9) are consistent with permeable compounds. In addition, the NMR solution structure of **1a** (Figure 1) in

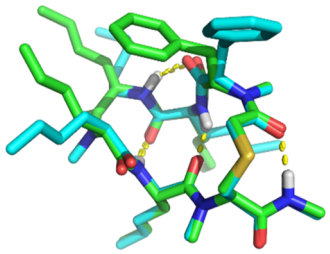

Figure 1. Overlay of calculated (green) and a representative experimentally determined (cyan) conformation of **1a** in low dielectric media.

chloroform (green) overlays well with the calculated conformation (cyan). A network of four intramolecular hydrogen bonds (two transannular and two extraannular) engages all four hydrogen-bond donors of **1a**, including the secondary amide NH of the C-terminal Cys. Overall, the low energy conformation of **1a** presents no hydrogen-bond donors to the solvent.

Likewise, for the remaining congeneric series in Table 1, the unmethylated parent examples **2**−**7** exhibit higher $\Delta G^*_{transfer}$ values and number of exposed backbone NHs, as well as lower PAMPA log P_{app} values than the corresponding methylated analogues. For example, methylated analogues **2a** and **2b** exhibit lower $\Delta G^*_{transfer}$ values (−7.55 and −5.78 kcal·mol^{-1}, respectively) and exposed hydrogen-bonds (0 and 1, respectively) than parent **2** ($\Delta G^*_{transfer}$ −4.45 kcal·mol^{-1} with two solvent-exposed backbone NHs). The higher measured permeability for **2a** and **2b** (PAMPA log P_{app} −4.6 and −5.1, respectively) than for parent **2** (PAMPA log P_{app} < −6.0) follows directly from the expectation set by the calculated values. Example **2c** ($\Delta G^*_{transfer}$ −4.26 kcal·mol^{-1}) highlights the number of solvent-exposed backbone NHs as an important predictor of permeability (PAMPA log P_{app} −5.1) relative to control **2**. Examples **2d** and **2e** lend further support to the trend. For Series C−G, we selected for synthesis N-methylated examples with both lower $\Delta G^*_{transfer}$ values and number of solvent-exposed backbone NHs; each pair mirrored the anticipated consequences on permeability.

A representative set of $\Delta G^*_{transfer}$ values for two of the ten congeneric series, Series A and B, are plotted *versus* the experimentally determined permeability in the PAMPA assay, as shown in Figure 2. In general, the lowest (most negative)

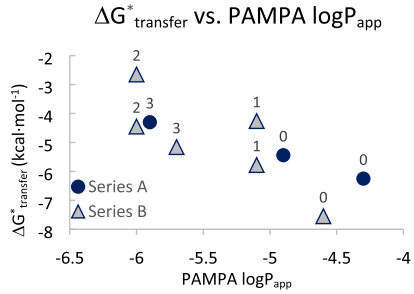

Figure 2. Calculated $\Delta G^*_{transfer}$ values and number of exposed NHs in lowest energy conformation for congeneric Series A and B.

$\Delta G^*_{transfer}$ values track with the predicted conformations with the lowest number of solvent-exposed backbone NHs. For example, low PAMPA permeability was observed for macrocycles with calculated conformations with ≥ two solvent-exposed backbone NHs; conversely, high PAMPA permeability is observed for those calculated conformations with no solvent-exposed NHs.

https://dx.doi.org/10.1021/acs.jmedchem.0c01505
J. Med. Chem. 2021, 64, 2622−2633

Measured log D (pH 7.4)[32] for the seven example compounds in Table 2 lie below calculated values by an average of 4.1 units, highlighting the risks of utilizing additive, calculated values to predict the properties of large compounds. Within each congeneric series, N-methylation increased log D (pH 7.4) by ~0.5 units, decreased EPSA by an average of 32 Å^2 (to below the proposed 80 Å^2 guidance),[33] and increased permeability in the MDCK-LE assay relative to the unmethylated comparator. Overall, examples in Table 2 showed high clearance in both human and rat liver microsomes and, excepting **7** and **7a**, low aqueous solubility.

Table 2. *In Vitro* ADME Data for 1, 1a, 1b, 2, 2a, 7, and 7a

	1	1a	1b	2	2a	7	7a
MW (g·mol^{-1})	774	816	802	774	802	758	800
clog P[a]	7.3	9.3	8.6	7.3	8.6	6.2	8.2
log D[b]	3.6	4.1	4.6	3.6	4.2	3.1	3.6
EPSA[c] (Å)^2	105	69	74	107	75	96	66
MDCK-LE[d] (×10^{-6} cm·s^{-1})	0.6	8.0	3.9	0.4	1.5	0.6	6.3
solubility[e] (μM)	<4	12	5	5	18	200	216
RLM and HLM Cl[f] (μL·min^{-1}·mg^{-1})	350 to >700						

[a]Calculated log P by the method available in ChemDraw 17.1. [b]Measured log D at pH 7.4 using the column-based method. [c]Experimental polar surface area (EPSA). [d]P_{app}A−B permeability in low efflux transporter expressing Madin−Darby canine kidney cells (MDCK-LE). [e]Aqueous solubility at pH 6.8. [f]Clearance in rat (RLM) and human liver microsomes (HLM).

Rat pharmacokinetic parameters for **1**, **1a**, **1b**, **7**, and **7a** are presented in Table 3. The oral exposure of **1** fell below the limit of quantitation (bql). Likewise, high clearance of **1** precluded calculation of its pharmacokinetic parameters. By contrast, the N-methylated congeners **1a** and **1b** achieve far higher systemic exposures, C_{max} (114 and 1028 nM, respectively) and AUC (258 and 2288 nM·h, respectively). Hepatic portal vein concentrations of **1a** or **1b** following oral administration reflect 67−100% of the systemic C_{max} and AUC values, suggesting that the ~20% F for **1a** and **1b** follows from low fraction absorbed rather than first pass metabolism. Despite uniformly high intrinsic clearance across the series (Table 2), the *in vivo* clearances of **1a** and **1b** differentiate from that of **1** and from each other. The lower clearances observed in the pharmacokinetic studies, which are lower than would be predicted by the liver microsomal data, may stem from their hydrophobicity, high plasma protein binding, and restricted access of the side chains to metabolic oxidation. In fact, the clearance of **1b** is only about 10% of the rate of hepatic blood flow in rats.[34] Pharmacokinetic parameters for **7** and **7a** match the expected trend, with higher systemic exposure and lower clearance observed for backbone methylated **7a** relative to parent **7**.

Table 3. Rat Pharmacokinetic Parameters for 1, 1a, 1b, 7, and 7a Dosed 5 mg/kg PO or 0.5 mg/kg IV

	1[c]	1a[d]	1b[d]	7[d]	7a[d]
systemic C_{max} (nM)	bql[a]	114	1028	1.7	152
hepatic portal vein C_{max} (nM)	nd[b]	140	819	nd[b]	nd[b]
systemic AUC (nM·h)	bql[a]	258	2288	0.6	92
hepatic portal vein AUC (nM·h)	nd[b]	173	1859	nd[b]	nd[b]
Cl (mL·min^{-1}·kg^{-1})	702 ± 239	86	8.9	222	72
$t_{1/2}$ (h)	0.3 ± 0.2	0.9	3.8	0.2	0.3
V_{ss} (L·kg^{-1})	nd[b]	2.1	1	2	1.3
% F	≪1	20	19	≪1	6

[a]Below the limit of quantitation. [b]Not determined. [c]n = 3. [d]n = 2.

Encouraged by the 6-mer results, we applied the $\Delta G^*_{transfer}$ and conformational analysis-based strategy to larger macrocycles, beginning with 7-mers containing 0−4 N-methylated residues. Overall, following the methods and design for the 6-mers, calculations were performed on a virtual library of 768 7-mer macrocyclic peptides. Based on the calculated values and conformations (plus reference controls), 10 peptides were selected for synthesis and profiled *in vitro* and *in vivo*. Results from a representative 7-mer congeneric series with Phe[1] and Pro[3] are shown in Table 4. For the 7-mers in Table 4, a larger disparity exists between the clog P and measured log D (average 4.6 units) than for the 6-mers in Table 1 (average 4.1 units). The N-methylated analogues **8a**−**c**, characterized by both lower $\Delta G^*_{transfer}$ and fewer number of exposed backbone NHs, reflect earlier observations that N-methylation decreases EPSA below 80 Å^2 and increases both log D and permeability relative to the unmethylated comparator **8**. However, the doubly N-methylated example **8a** (AA^2, AA^4 = Nle) minimally impacts $\Delta G^*_{transfer}$ and leaves a residual solvent-exposed backbone NH. Therefore, example **8a**, with improved PAMPA permeability *versus* **8**, shows lower permeability relative to the examples **8b**, **c** (AA^2, AA^4, and AA^6 = Nle). Example **8c**, a representative aromatic side chain Phe, replaces the aliphatic Nle of **8b** with minimal impact on the profile. For both 6- and 7-mer series, we found that PAMPA and MDCK-LE values were generally correlated (Supporting Information Figure 1). The present data suggest EPSA ≤ ~80 Å^2 as an independent predictor of permeability. However, an expanded set of Novartis peptides show that EPSA ≤ ~80 Å^2 must be

Table 4. Profiling Data for 7-mers 8 and 8a−c

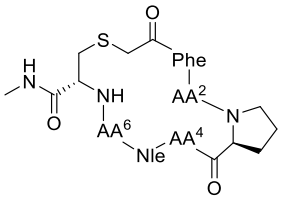

	AA^2	AA^4	AA^6
8	Nle	Nle	Nle
8a	Nle	Nle	Nle
8b	Nle	Nle	Nle
8c	Nle	Phe	Nle

	8	8a	8b	8c
$\Delta G^*_{transfer}$ (kcal·mol^{-1})	−2.37	−2.49	−4.12	−4.96
exposed NHs (count)	2	1	0	0
MW (g·mol^{-1})	871	899	913	947
clog P[a]	7.9	9.2	9.8	9.6
log D[b]	3.7	4.7	4.8	4.9
EPSA[c] (Å^2)	91	77	69	81
PAMPA log P_{app}	−6.2	−5.3	−4.0	−4.4
MDCK-LE[d] P_{app} A−B (×10^{-6} cm·s^{-1})	0.2	0.8	6.4	2.3
solubility[e] (μM)	9−24			
RLM and HLM Cl[f] (μL·min^{-1}·mg^{-1})	480 to >700			

[a]Calculated log P by the method available in ChemDraw 17.1. [b]Measured log D at pH 7.4 using the column-based method. [c]Experimental polar surface area (EPSA). [d]P_{app}A−B permeability in low efflux transporter expressing Madin−Darby canine kidney cells (MDCK-LE). [e]Aqueous solubility at pH 6.8. [f]Clearance in rat (RLM) and human liver microsomes (HLM).

https://dx.doi.org/10.1021/acs.jmedchem.0c01505
J. Med. Chem. 2021, 64, 2622−2633

combined with a minimum lipophilicity (log D) to achieve passive membrane permeability (Supporting Information Figure 2).

Rat pharmacokinetic parameters for 7-mers **8** and **8a**–**c** are presented in Table 5. Like **1** and **7**, unmethylated parent **8**

Table 5. Rat Pharmacokinetic Parameters for 8 and 8a–c Dosed 5 mg/kg PO or 0.5 mg/kg IV

	8[a]	8a[b]	8b[b]	8c[b]
systemic C_{max} (nM)	bql	18	868	1946
systemic AUC (nM·h)	bql	10	2130	1308
Cl (mL·min^{-1}·kg^{-1})	72 ± 21	106	35	19
$t_{1/2}$ (h)	0.08 ± 0.04	0.7	0.6	1.5
V_{ss} (L·kg^{-1})	0.2 ± 0.05	4.4	1.2	1.1
% F	≪1	1	86	84

[a]n = 3. [b]n = 2.

shows no/weak systemic exposure following oral dosing and short half-life ($t_{1/2}$ 0.08 ± 0.04 h) following IV administration. Example **8a** shows detectable oral exposure, but both **8b** and **c** (MW 913 and 947 g·mol^{-1}, respectively; clog P 9.8 and 9.6, respectively) show ∼85% F in the context of low/moderate clearance. Again, the *in vivo* rank order is best predicted by $\Delta G^{*}_{transfer}$, number of exposed backbone NHs, and consequent relative *in vitro* permeability, rather than molecular weight, clog P, log D, or liver microsome stability.

To explore the oral exposure of **8b** in nonrodent species, we assessed its pharmacokinetic profile in dogs (Figure 3).

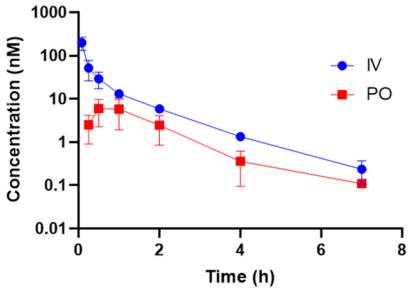

Figure 3. Intravenous and oral exposure profiles for **8b** in beagle dog (n = 3).

Macrocycle **8b** was dosed 0.1 mg/kg IV or 0.5 mg/kg PO in 5% neat solutol and 95% PBS. Following the IV dose, the clearance (24 ± 6 mL·min^{-1}·kg^{-1}) was moderate relative to liver blood flow[34] and the half-life was 1.1 ± 0.3 h. Following the PO dose, a fraction of the compound was rapidly absorbed, reaching a C_{max} of 6 ± 4 nM at a T_{max} of 0.7 ± 0.3 h. The oral bioavailability was only 3 ± 2%. This may be due to the strong efflux observed in a Caco-2 permeability assay (efflux ratio >25) reducing the amount absorbed in the dog at a low dose while the 10× higher dose in rat could have saturated the efflux transporter.

With successful identification of oral 7-mers, we further expanded our studies to 8-mers by selecting from 1514 virtual compounds with 0–4 N-methylated residues. In Table 6 are shown two congeneric series, marked by either Phe (**9**) or phe (**10**) at the N-terminal amino acid residue and no Pro residues. For each series, an N-methylation pattern predicted by *in silico* methods to have no exposed backbone NHs were prepared as **9a** and **10a**, respectively. Thereafter, additional side chain variants of **10a** were prepared as **10b** (AA^7 = Phe) and **10c**

Table 6. Structures of 8-mers 9, 9a, 10, and 10a–c

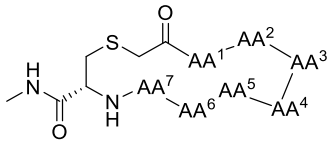

	AA^1	AA^2	AA^3	AA^4	AA^5	AA^6	AA^7
9	Phe	Nle	Nle	Nle	Nle	Nle	Nle
9a	Phe	Nle	Nle	Nle	Nle	Nle	Nle
10	phe	Nle	Nle	Nle	Nle	Nle	Nle
10a	phe	Nle	Nle	Nle	Nle	Nle	Nle
10b	phe	Nle	Nle	Nle	Nle	Nle	Phe
10c	phe	Thr	Nle	Nle	Nle	Nle	Phe

(AA^2 = Thr, AA^7 = Phe) to briefly explore the impact of the side chain on properties.[35–37]

Calculated, *in vitro*, and *in vivo* properties for **9a** and **10a**–**c** are presented in Table 7. For comparison, their unmethylated

Table 7. *In Vitro* and Rat *in Vivo* Pharmacokinetic Profile for 9a and 10a–c

	9a	10a	10b	10c
$\Delta G^{*}_{transfer}$ (kcal·mol^{-1})	−9.98	−9.69	−9.82	−7.27
exposed NHs (count)	0	0	0	0
MW (g·mol^{-1})	1056	1042	1076	1064
clog P	13	13	12	10
log D	6.1	6.0	6.2	5.2
EPSA (Å^2)	nd	73	85	86
MDCK-LE P_{app} A–B (×10^{-6} cm·s^{-1})	<0.35			
solubility (μM)	<4			
RLM/HLM Cl (μL·min^{-1}·mg^{-1})	120 to >700			
C_{max} (nM)[a]	436	411	77	161
AUC (nM·h)[a]	1077	1269	237	372
Cl (mL·min^{-1}·kg^{-1})[a]	12	33	65.4	28.4
% F[a]	17	54	21	13

[a]n = 2.

parent scaffolds **9** and **10** had calculated $\Delta G^{*}_{transfer}$ values in the range of −7 to −8 kcal·mol^{-1} and at least three solvent-exposed backbone NHs. Each N-methylated example in Table 7 exceeds 1000 g·mol^{-1} molecular weight and calculated log P values of 10, but is consistent with no exposed backbone NHs. Not unexpectedly, measured log D values at pH 7.4 (all ≥5.2) exceed the values reported above for the 6- and 7-mers and reflect the largest gap from the calculated values (average 6.1 units). Compound **10a** achieves EPSA below 80 Å^2, in line with guidance for peptides with passive permeability, with values near 80 Å^2 for **10b** and **10c** (85 and 86 Å^2, respectively).

However, compounds **10a**–**c** show undetectable P_{app} A–B in the MDCK-LE assay (with ≥67% recovery) and consistently poor stability in liver microsomes. All four examples in Table 7 are orally exposed at levels consistent with a subset of potential therapeutic applications. Furthermore, despite their high intrinsic clearance, three of the four examples (**9a**, **10a**, and **10c**) show low to moderate clearance in rats. Compounds **10a**–**c**, which share identical backbone N-methylation patterns and vary only by side chain identity, illustrate the potential for expanding validated N-methylated backbones to larger families of orally exposed analogues.

https://dx.doi.org/10.1021/acs.jmedchem.0c01505
J. Med. Chem. 2021, 64, 2622–2633

CONCLUSIONS

We show that multiple series of orally exposed cyclic peptides with MWs at and above 1 kDa can be reliably identified by 3D physics-based *in silico* methods in advance of chemical synthesis. By contrast, standard 2D *in silico* descriptors (*e.g.*, MW, clog *P*, and TPSA) that neglect 3D macrocycle conformation, used alone or in combination, poorly predict macrocycle permeability and oral exposure. Like rule-compliant, orally exposed small molecules,[38] orally exposed macrocycles balance lipophilicity and polar surface area, properties that can be assessed using measured log *D* and EPSA, respectively. However, due caution is warranted when utilizing strict cutoffs. For the largest, most lipophilic oral macrocycles examined, log *D* and EPSA exceed proposed limits. In advance of chemical synthesis, $\Delta G^*_{transfer}$ and number of solvent-exposed polar groups, respectively, can focus synthetic efforts on compounds with balanced log *D* and EPSA.

Despite the kinetic nature of permeability and complexity of oral bioavailability, it is remarkable that the combination of 3D physics-based predictors, such as $\Delta G^*_{transfer}$ and number of solvent-exposed hydrogen-bond donors, can identify permeable and orally bioavailable macrocycles. The data support combining $\Delta G^*_{transfer}$ calculations with conformational analysis to select compounds with favorable $\Delta G^*_{transfer}$ values and minimal number of solvent-exposed hydrogen-bond donors. Further efforts are needed to enable quantitative comparison across noncongeneric series. Recent advances in macrocyclic sampling[39,40] and structure-kinetic simulation studies[41] of passive membrane simulations should facilitate this and provide insights into descriptors suitable for high-throughput permeability predictions.

Adding to the body of existing knowledge, these data illustrate further that privileged N-methylated peptide backbones, whether identified by Nature, by serendipity, or by design, can seed families of oral peptides. Families of permeable peptides share common peptide backbones and N-methylation patterns, which reduce polar surface area, drive macrocycle conformation, and set the intramolecular hydrogen-bond network. No doubt, permeability can be overwhelmed by side chains with limited hydrophobicity, high polarity, and/or charge. However, the available diversity of lipophilic, noncanonical side chains alone is vast. Reports describing permeable peptides bearing polar side chains[35] add further opportunity. In addition, as Nature shows, there is utility at the intersection of passively permeable peptides and challenging protein surfaces. While the rat oral exposures of many of the examples contained herein do not meet the levels commonly achieved by standard small molecules, a subset of compounds, especially **1b**, **8b**, and **10a**, offer impressive rat exposure relative to most peptides. We do note that the predictability of the rat oral data to higher species may be variable. Nonetheless, the oral exposures achieved herein may be suitable for a subset of therapeutic applications in humans, including protein surfaces that are especially challenging for traditional, rule-compliant small molecules. It should also be noted that several of the examples presented herein, such as **8b**, inhibit CYP3A4 (IC_{50} 370 nM), a property shared by other lipophilic macrocycles such as 1NMe3 (IC_{50} 3640 nM) and CsA (IC_{50} 1500 nM), so potential for drug−drug interaction in a therapeutic setting must also be considered. Finally, the potential of large array library formats, including *in vitro* translation methods, to effect the synthesis of families of macrocycles with preset N-methylation patterns link property/permeability-biased structure design with powerful ligand identification technology, an important step toward identifying passively permeable ligands to therapeutically relevant protein targets.

EXPERIMENTAL SECTION

Modeling and Simulation Details. The sequences of all possible N-methylated variants with 0−3, 4, or 4 N-methylated residues (not counting Pro) were generated for each of 10, 12, or 14 scaffolds for 6-mers, 7-mers, and 8-mers, respectively, using in-house Perl script. This resulted in 292, 768, and 1514 sequences of virtual peptides, respectively. The initial conformers for all-atom models of these peptides were generated *via* LEaP program in AmberTools12[42] based on manually created poly Ala 6-mer, 7-mer, and 8-mer templates and using the Amber99sb[43] force field with the parm@Frosst[44] small-molecule extension and AM1-BCC[45] charges. The resulting initial conformers were minimized with Sander program in AMBER 12[42] to relax the side chains; restraints were applied to prevent chirality inversions. The minimized structures were converted to Maestro format by Protein Preparation Wizard from Schrödinger software package[46] for further calculations with MacroModel.[47]

We adapted the published approach to passive permeability predictions from Jacobson's group[31] and complemented it with intramolecular hydrogen-bonding analysis. We focused on transfer free energy from water to membrane ($\Delta G_{transfer}$ and $\Delta G^*_{transfer}$) as a dominant factor for permeability. This is because (a) the studied compounds are charge neutral and exist as a single tautomer and, therefore, the free energy penalty for our compounds to adopt their neutral form for membrane permeation is zero; (b) our comparisons were done within each of the congeneric series and, therefore, based on their work,[31] the permeant size effect on permeability was expected to be small for that purpose. An approximate transfer free energy from water to membrane was computed as follows. Conformations within 5 kcal/mol were generated in low dielectric media (LDM, the dielectric constant of chloroform), mimicking the cell membrane inner hydrophobic layer. Conformations in high dielectric media (HDM, representing water) were generated for a few cases initially as well but were found not necessary for our studies and not pursued further. Generalized Born (GB)[48−54] implicit solvation models for chloroform and water were used for LDM and HDM, respectively. $\Delta G_{transfer,i}$ was approximated by its energy difference between LDM and HDM for ith conformation; $\Delta G_{transfer}$ was for the lowest energy conformer (see also ensemble-based $\Delta G^*_{transfer}$ below). The conformation generation was performed with macrocycle conformational sampling script in MacroModel, which combines simulated annealing with large-scale low-mode conformational search; we used optimal parameters previously described[47] (10,000 search cycles, 10 kcal/mol energy window, recalculating the eigenvectors when a new global energy minimum is found). The resulting conformations were clustered with the cutoff of 0.75 Å.

The 6-mers selection was done as follows. The top 2−4 peptides from each scaffold with the lowest $\Delta G_{transfer}$ were selected for synthesis and the conformations of these peptides were examined to make sure that all backbone NHs were paired with backbone carbonyls in at least some of them. $\Delta G_{transfer}$ was calculated for all generated conformations and the lowest $\Delta G_{transfer}$ was recorded from an ensemble ($\Delta G^*_{transfer}$) and the corresponding conformation was analyzed. The conformations for selected peptides were sampled with both OPLS2005[55] and MMFF94s[56] force fields. In addition, mutants that were trimmed to Ala at each residue were simulated as well to improve overall sampling.

The 7-mers and 8-mers selections were done similarly to 6-mers, but in addition, $\Delta G_{transfer}$ for each peptide was calculated for all generated conformations and the lowest $\Delta G_{transfer}$ was recorded from an ensemble ($\Delta G^*_{transfer}$). For the 7-mers, the corresponding conformations were examined to make sure that backbone NHs were paired with backbone carbonyls as much as possible, and these

https://dx.doi.org/10.1021/acs.jmedchem.0c01505
J. Med. Chem. 2021, 64, 2622−2633

compounds were selected for synthesis. For the 8-mers, we restricted synthesis to only compounds that had all backbone NHs paired with backbone carbonyls.

NMR Experimental Details. Compound **1a** was dissolved in 50 μL of $CDCl_3$ and placed in a 1.7 mm NMR tube. The tube was purged with nitrogen gas before and after the sample delivery and sealed with Parafilm. All data were recorded on a Bruker 600 MHz (for 1H) AVANCE III spectrometer equipped with a 1.7 mm TCI cryoprobe. Data analysis was done using Mnova software. Resonance assignments, ROESY cross peak assignments, and integrations were carried out manually. The mixing time used for the ROESY spectrum was 400 ms. ROESY peak integrals were qualitatively categorized as weak, medium, or strong and are listed in Supporting Information Table 1, with the corresponding atom numbers in Supporting Information Figure 3. This table was used for NMR structural refinements. Two conformers were observed in the NMR spectra in a ~60:40 ratio at 300 K and only the peaks from the major conformer were used in the modeling.

NMR Structural Refinements. An all-atom model of **1a** was built as previously described above. The respective topology and coordinate files were generated *via* LEaP program in AmberTools12 using Amber99sb force field with the parm@Frosst small-molecule extension and conformationally and topologically averaged AM1-BCC charges.

Molecular dynamics simulations in implicit solvent (Generalized Born model)[57] were run with the Sander program in AMBER 12. The dielectric constant of the solvent was 4.8, corresponding to chloroform. The temperature was controlled using a Langevin thermostat with a collision frequency of 5 ps^{-1}.

The system was first subjected to a 5000 step minimization (300 steps by the steepest descent followed by the conjugate gradient method) followed by 50 independent 700 ps simulated annealing runs with restraints based on ROE data (Supporting Information Table 1). Each simulated annealing run consisted of heating from 0 to 1200 K for 200 ps, followed by equilibration at 1200 K for 200 ps and then cooling to 600 K and then to 300 K for 100 ps, followed by further cooling from 300 to 0 K for 200 ps; the restraints were gradually turned on for the first 400 ps and stayed on till the end of the simulation. The resulting ensemble of structures was clustered and selected based on the smallest number of ROE violations.

Cyclic Peptide Synthesis. A general synthetic scheme for 6-mer compounds is shown in Scheme 1, and 7-mer and 8-mer compounds were prepared in an analogous manner. All chemicals and resins were commercially available and used without further purification or prepared as indicated. All amino acid building blocks used were Fmoc-protected. Anhydrous solvents were obtained from Sigma-Aldrich and used as received. Reactions were monitored using LCMS, and products were purified using reverse-phase preparative HPLC, followed by lyophilization.

Automated Peptide Synthesis. All peptides were synthesized on the Liberty peptide synthesizer from CEM, Inc. Peptides were synthesized on a 0.1 mmol or 0.25 mmol scale, starting from Methyl Indole AM resin obtained from EMD Millipore. Either Fmoc-Cys(Trt)-OH or Fmoc-Cys(Mtt)-OH was used to introduce the initial cysteine residue. Fmoc deprotection was achieved in two cycles of treatment with 4-methylpiperidine, the first for 30 s, and the second for 3 min. All amino acids were activated with HATU and Hunig's base. At a 0.1 mmol scale, 5 equiv of the amino acid were used; at a 0.25 mmol scale, 4 equiv were used. All amino acids were coupled for 10 min at 75 °C, except for cysteine, which was coupled for 10 min at 50 °C. After the peptide synthesis was complete, the resins were filtered and washed twice each with dimethylformamide and dichloromethane and dried under house vacuum.

Peptide Acylation and Deprotection. The resin was suspended in *N*-methylpyrrolidine (3−8 mL), and 5 equivalents of *N*-(chloroacetoxy)succinimide (prepared as described below) were added. The resulting resin mixture was shaken at room temperature overnight. The following morning, the resin was filtered, washed three times each with dimethylformamide and dichloromethane, and then dried under house vacuum. The resin was then treated for 1 h with a cleavage cocktail consisting of TFA/H_2O/TIS 92.5:2.5:5 (3−5 mL). The resin was filtered and treated again with cleavage cocktail (2−3 mL) for 30 min. The resin was filtered and the combined filtrates were concentrated to yield the crude linear peptide.

***N*-(Chloroacetoxy)succinimide Preparation.** To a stirred suspension of 1-hydroxypyrrolidine-2,5-dione (30 g, 261 mmol) in dichloromethane (300 mL) cooled to 0 °C was added solid sodium bicarbonate (32.8 g, 391 mmol), followed by 2-chloroacetyl chloride (22.81 mL, 287 mmol) slowly at 0 °C. The ice bath was removed and the reaction mixture was then stirred at room temperature for 2 h. Sodium sulfate (20 g) was added to the reaction mixture and the resulting mixture was filtered. The filtrate was evaporated *in vacuo*. The residue was triturated with ethyl acetate/heptane 1:1 (120 mL) to provide *N*-(chloroacetoxy)succinimide (36.4 g, 190 mmol, 72.9% yield), whose analytical data matched with the literature.[58]

Peptide Cyclization. The crude peptide was dissolved in dimethylsulfoxide (5−8 mL) and treated with triethylamine until a pH of 9 was obtained by pH paper (typically *ca.* 200−500 μL of triethylamine). The reaction mixture was then shaken overnight at room temperature. The following morning, the product mixture was concentrated on a GeneVac to a few milliliters of solution and was directly purified in 1−1.5 mL injection aliquots onto a reverse-phase preparative HPLC Waters Autopure with UV-MS detection, a flow rate of 75 mL/min, outfitted with either 30 × 50 Waters Sunfire C18 5 μm column (ACN and water with a 0.1% TFA modifier) or 30 × 50 Waters XBridge C18 5 μm column (ACN and water with 5 mM ammonium hydroxide). Desired fractions were collected, triggering either by absorption at 210 nm or by mass spectrometry, and lyophilized to yield the final products.

Compound Characterization Data. All peptides were characterized as ≥95% purity by either UPLC or HPLC (traces provided in Supporting Information Figure 4). Table 8 indicates for each product

Table 8. Characterization Data for Compounds 1−10c

compound no	retention time	analytical method	HRMS calculated	HRMS found
1	3.12	A	NA	774.4[c]
1a	2.94	G	816.5057	816.5020
1b	3.03	C	802.4900	802.4854
2	1.34	F	774.4615	774.4623
2a	2.99	C	800.4744	800.4742
2b	4.48	B	802.4900	802.4908
2c	3.18	C[a]	816.5057	816.5040
2d	2.82	C	802.4901	802.4904
2e	2.94	C	788.4744	788.4805
3	2.48	D	758.4274	758.4288
3a	2.66	G	800.4744	800.4788
4	2.35	D	758.4276	758.4275
4a	2.43	C	772.4431	772.4491
5	2.38	C	NA	758.9[c]
5a	2.73	G	800.4744	800.4742
6	2.92	A	NA	759.0[c]
6a	2.85	G	800.4744	800.4815
7	2.50	C	758.4275	758.4315
7a	2.74	C	800.4744	800.4748
8	2.66	D	871.5116	871.5119
8a	3.11	C[b]	899.5428	899.5476
8b	3.13	C	NA	913.9[c]
8c	1.47	F	947.5428	947.5507
9a	2.81	E	1055.6817	1055.6816
10a	2.81	E	1041.6660	1041.6660
10b	1.61	F	1076.6582	1075.6504
10c	1.51	F	1064.6218	1064.6285

[a]Poor UV chromophore, purity assessed by ELSD. [b]Column contained a UV-active contaminant, purity assessed by CAD. [c]LRMS.

https://dx.doi.org/10.1021/acs.jmedchem.0c01505
J. Med. Chem. 2021, 64, 2622−2633

the analytical method used to determine retention time and purity, which was assessed by UV absorption at 214 nm unless otherwise indicated. HRMS data were obtained on a Waters AcQuity UPLC using either a Waters LCT Premier or Waters Xevo G2 Qtof detector. For a few peptides where indicated, HRMS data were not obtained, and so LRMS data are provided. The analytical method descriptions are listed below.

Method A—Instrument: Agilent 1100/1200 HPLC; column: XBridge C18 3.5 μm 3.0 × 30 mm; 5.10 min run time, 5 → 80% solvent B: solvent A from 0 to 4.30 min, 80 → 95% solvent B: solvent A for 0.4 min, 95% solvent B for 0.3 min, 95 → 5% solvent B: solvent A for 0.1 min. Solvents: solvent A = 5 mM ammonium hydroxide in water, solvent B = acetonitrile. UV detection array 210−400; mass detection 150−1600; column at 40 °C; flow rate 2.0 mL/min; pH 10.2.

Method B—Instrument: Waters AcQuity UPLC; column: AcQuity UPLC BEH C18 1.7 μm, 2.1 × 50 mm; 8.05 min run time, 2 → 98% solvent B: solvent A from 0 to 7.5 min, 98% solvent B for 0.4 min, 98 → 2% solvent B: solvent A for 0.15 min. Solvents: solvent A = 5 mM ammonium hydroxide in water, solvent B = 5 mM ammonium hydroxide in acetonitrile. UV detection array 210−400; mass detection 120−1250; column at 50 °C; flow rate 1.0 mL/min; pH 10.2.

Method C—Instrument: Waters AcQuity UPLC; column: AcQuity UPLC BEH C18 1.7 μm, 2.1 × 50 mm; 5.19 min run time, 2 → 98% solvent B: solvent A from 0 to 4.40 min, 98% solvent B for 0.75 min, 98 → 2% solvent B: solvent A for 0.04 min. Solvents: solvent A = 0.1% formic acid in water (v/v), solvent B = 0.1% formic acid in acetonitrile (v/v). UV detection array 210−400; mass detection 120−1250; column at 50 °C; flow rate 1.0 mL/min; pH 2.6.

Method D—Instrument: Waters AcQuity UPLC; column: AcQuity UPLC BEH C18 1.7 μm, 2.1 × 50 mm; 5.19 min run time, 2 → 98% solvent B: solvent A from 0 to 4.40 min, 98% solvent B for 0.75 min, 98 → 2% solvent B: solvent A for 0.04 min. Solvents: solvent A = 5 mM ammonium hydroxide in water, solvent B = 5 mM ammonium hydroxide in acetonitrile. UV detection array 210−400; mass detection 120−1250; column at 50 °C; flow rate 1.0 mL/min; pH 10.2.

Method E—Instrument: Waters AcQuity UPLC; column: AcQuity UPLC BEH C18 1.7 μm, 2.1 × 50 mm; 8.05 min run time, 40→98% solvent B: solvent A from 0 to 5.00 min, 98% solvent B for 2.09 min, 98 → 40% solvent B: solvent A for 0.06 min. Solvents: solvent A = 0.1% formic acid in water (v/v), solvent B = 0.1% formic acid in acetonitrile (v/v). UV detection array 210−400; mass detection 125−1200; column at 50 °C; flow rate 1.0 mL/min; pH 2.6.

Method F—Instrument: Waters AcQuity UPLC; column: AcQuity UPLC CSH 1.7 μm, 2.1 × 50 mm; 2.2 min run time, 2% solvent B, from 0 to 0.6 min, 2 → 98% solvent B/solvent A for 1.7 min, 98% solvent B for 0.24 min, 98 → 2% solvent B/solvent A for 0.16 min. Solvents: solvent A = 0.05% trifluoroacetic acid in water (v/v), solvent B = 0.05% trifluoroacetic acid in acetonitrile (v/v). UV detection array 210−400; mass detection 100−2050; column at 50 °C; flow rate 1.0 mL/min; pH 2.6.

Method G—Instrument: Waters AcQuity UPLC; column: AcQuity UPLC BEH C18 1.7 μm, 2.1 × 50 mm; 5.19 min run time, 2 → 98% solvent B: solvent A from 0 to 4.40 min, 98% solvent B for 0.75 min, 98 → 2% solvent B: solvent A for 0.04 min. Solvents: solvent A = 0.1% formic acid in water (v/v), solvent B = 0.1% formic acid in acetonitrile (v/v). UV detection array 210−400; mass detection 200−2000; column at 50 °C; flow rate 1.0 mL/min; pH 2.6.

Profiling and Pharmacokinetic Experiments. *In vitro* ADME, physicochemical, and pharmacokinetic profiling was conducted by published methods or modifications to published methods. All animal experiments performed in the manuscript were conducted in compliance with institutional guidelines.

Log *D* Method. Phosphate-buffered saline (pH 7.4) saturated with 1-octanol and 1-octanol saturated with buffer was prepared prior to the start of the log *D* assay. Aliquots of 10 mM DMSO compound solution along with an internal reference compound were dispensed in triplicate in 96-well polypropylene 2 mL plates. The DMSO was removed under temperature and vacuum.

Dried samples were incubated with 300 μL of octanol and 300 μL of buffer and shaken for at least 4 h. Plates were centrifuged for 15 min at 4000 rpm to separate the octanol and buffer layers. Sample preparation and phase separation were automated using liquid handling workstations. Both octanol and buffer phases were quantified using liquid chromatography with tandem mass spectrometry. Log *D* was derived from the ratio of compound peak area responses in each phase, adjusted to the internal standard peak areas.

EPSA Method. Analysis for the determination of the experimentally derived polar surface analysis value (EPSA) was performed using a modified set of conditions from those previously described.[33,59] The sample was dissolved to an approximate concentration of 5 mM in DMSO. Analysis was performed on the Waters Acquity UPC2 supercritical fluid chromatography system with a photodiode array and a Waters QDa mass spectrometer with a single quadrupole (Milford, MA). The mobile phase consisted of two parts. Mobile phase A consisted of carbon dioxide pressurized to 850 psi using a Waters Bulk Delivery System (BDS). Mobile phase B was ammonium formate diluted to 20 mM in HPLC-grade methanol.

Analysis was performed using a 4.6 mm × 250 mm Chirex 3014 column (Phenomenex, Torrance, CA) with 5 μm particle size and 100 Å pore size. The flow rate was 3 mL/min with an automated back pressure regulator set point of 2100 psi. Each injection was performed using an injection volume of 3 μL. The column temperature set point during the analysis was 40 °C. The composition of the mobile phase was varied linearly from 5 to 65% mobile phase B over 4.6%/min, holding at 65% for 2 min, and then reverting to the original 5% until the end of the run with a total data acquisition time of 19 min.

MDCK-LE Method.[60] MDCK-LE (low efflux) cells were cultured at 37 °C under a 5% CO_2 atmosphere, at 95% relative humidity in DMEM containing 10% FBS, penicillin−streptomycin (100 μg/mL), and 2 mM Ala−Gln. Cells were passaged every 3−4 days. For assay purposes, cells were seeded at a density of approximately 265,000 cells/cm^2 of a 96-well Transwell plate (Corning Life Sciences, Acton, MA) and cultured in the same media noted above for a period of 4 days.

Assay. The determination of the apparent permeability (Papp) was performed in the A → B (apical to basal) direction where each compound was assayed in triplicate. The zwitterion bestatin, a poorly permeably compound, was used as a marker of monolayer integrity. To initiate the assay, media was aspirated, and the cells and basal chambers were washed three times with Hank's Balanced Salt Solution (HBSS) containing 10 mM HEPES (pH 7.4). Compound test solutions were prepared in triplicate in HBSS containing 10 mM HEPES (pH 7.4) and 0.02% bovine serum albumin (BSA) to a final concentration of 10 μM and centrifuged for 2 min at 4000*g* and then applied to the donor compartment at time zero. Additionally, at time zero, a 37 °C solution without test articles [HBSS + 10 mM HEPES (pH 7.4) plus 0.02% BSA] was added to the receiver chamber of the Transwell plate. A time zero sample of the donor solution was also sampled for further analysis. The assay was conducted for a period of 120 min at 37 °C without shaking. At the time of assay termination, samples were taken from each donor compartment and each acceptor compartment of the Transwell plate. To each of the 0 and 120 min samples was added an internal standard solution containing glyburide in water: acetonitrile, 50:50 (v/v). Concentration curves were prepared using a Labcyte Echo in the same matrix noted above. Samples and concentration curve samples were centrifuged for 10 min at 4000*g* and subsequently analyzed by mass spectroscopy.

Mass Spectrometry. Assay samples were loaded onto a RapidFire C4 cartridge by means of a RapidFire autosampler (Agilent, Santa Clara, CA). Chromatography was performed at a flow rate of 1.25 mL/min, loading with 0.1% formic acid in water, and eluting in 0.1% formic acid in methanol. Mass spectroscopy was performed using an AB Sciex API5500 (Sciex, Framingham, MA) equipped with a turbo ion spray source. The analyte concentration was calculated from the chromatographic peak area ratio of the analyte to internal standard

https://dx.doi.org/10.1021/acs.jmedchem.0c01505
J. Med. Chem. 2021, 64, 2622−2633

(glibenclamide, m/z 494 → 169), using Multiquant software V3.0 (Sciex, Framingham, MA).

Calculations. Papp values were determined as

$$P_{app} = VA/(S[D_0]) \times A_{120}/t$$

Percent recovery values were determined as

$$\% \text{ recovery} = 100 \times ((A_{120} + D_{120})/D_0)$$

where VA is the volume of the acceptor (mL), S is the surface area of the membrane, D_0 is the donor solution concentration at $t = 0$, D_{120} is the donor solution concentration at $t = 120$, A_{120} is the acceptor solution concentration at $t = 120$, and t = time (seconds).

High-Throughput Equilibrium Solubility. The high-throughput (HT) equilibrium solubility assay was performed as previously described.[61] Briefly, aliquots of 10 mM DMSO stock solution were plated and DMSO was removed under temperature and vacuum. Media (pH 4.0 acetate buffer, pH 6.8 phosphate buffer, or FaSSIF-v2: Fasted State Simulated Intestinal Fluid) was added to the 96-well plate for a target concentration of 1 mM. The plate was sealed, incubated on a shaker at 1350 rpm and ambient temperature for 16–24 h, and then centrifuged for 20 min at 3750 rpm to pellet the precipitate. The supernatant was transferred to another plate and centrifuged a second time. The supernatant was diluted 200-fold with 50:50 acetonitrile/water and a 4-point calibration curve was constructed using 50:50 acetonitrile/water. Analysis of the supernatant concentration was performed based on the calibration curve, using an Agilent RapidFire-MS/MS mass spectrometer system.

Human Microsomal Incubations. The experiments were performed in 96-well format with shaking incubation at 37 °C on an automated platform. Test articles, at a concentration of 10 mM in DMSO, were diluted 1:1000 into a 100 mM potassium phosphate solution to a concentration of 10 μM. This solution was added to human liver microsomal protein (1.25 mg/mL) suspended in phosphate buffer (pH 7.4). The assay reactions were initiated by the addition of a cofactor solution (2 mM NADPH, 4 mM $MgCl_2$ in 100 mM potassium phosphate). At specific reaction time points (0, 5, 15, and 30 min), reaction aliquots were removed and reactions were terminated by the addition of three volumes of acetonitrile containing the analytical internal standard (glibenclamide). The samples were then centrifuged at 4000g at 4 °C for 10 min, and the supernatants were analyzed by LC/MS/MS for quantitation of the remaining test article. The percentage of test article remaining, relative to time zero minute incubation, was used to estimate the *in vitro* elimination-rate constant (kmic), which was subsequently used to calculate the *in vitro* metabolic clearance rates.

LC/MS/MS Analysis. Analysis of samples was performed on a high-performance liquid chromatography (HPLC)-tandem mass spectrometry (LC/MS/MS) system consisting of a Shimadzu 30 series autosampler and HPLC pump coupled to an AB Sciex API6500. Compound-specific parameters (precursor ion, product ion, declustering potential, and collision energy for single reaction monitoring) were obtained by automatic tuning using the Multiquant software V3.0. Samples were injected onto a 3 μm ACE 3 C18, 2.1 mm × 30 mm column, by means of the Shimadzu 30 series autosampler. The components were eluted with a gradient of 0.1% formic acid (mobile phase A) and 0.1% formic acid in acetonitrile (mobile phase B) at a flow of 700 μL/min using the following gradient: 0 min 2% B; 0.25 min 2% B; 1.00 min 98% B; 1.55 min 98% B; 1.95 min 2% B; 2.00 min 2% B. The analyte concentration was calculated from the chromatographic peak area ratio of the analyte to an internal standard (glibenclamide, m/z 494 → 169), using Multiquant software V3.0 (Sciex, Framingham, MA).

Ethics Statement. All *in vivo* research was reviewed and approved by the Novartis Institutes of Biomedical Research Institutional Animal Care and Use Committee in accordance with applicable local, state, and federal regulations.

Pharmacokinetic Studies in Rat. PK studies in rat were conducted either at Charles River laboratories (Worchester, MA 01605) or internally at Novartis. Studies were conducted in male Sprague–Dawley rats (age approximately 9–11 weeks, weight approximately 300–325 g, n = 2 or 3). The compounds were formulated in solution in PEG300: 20% Solutol/PBS (10:25:65) and dosed intravenously (IV, *via* injection into the jugular vein cannula) at a dose of 0.5 mg/kg (compounds **1**, **1a**, **1b**, **7**, **7a**, **8a**, **8b**, **9a**, and **10a**) or 1 mg/kg (compounds **8**, **8c**, **10b**, and **10c**) with a dosing volume of 1 mL/kg. Compounds were formulated in solution at 0.5 mg/mL in the same formulation for PO dosing (PO, *via* oral gavage; at 5 mg/kg). Approximately, 100 μL of whole blood was collected from each animal *via* a jugular vein cannula at 5 min (IV dose only), 15 min, 0.5, 1, 2, 4, 7, and 24 h post-dose and transferred to EDTA tubes. Blood samples were centrifuged at 3000 rpm and the resultant plasma was transferred to a capped PCR 96-well plate and frozen at −20 °C until subsequent preparation and analysis by HPLC-MS/MS.

Pharmacokinetics Study in Dogs. The dog PK study was conducted at Agilux (One Innovation Drive, Worchester, MA 01605). The pharmacokinetics of compound **8b** was determined in male beagle dogs (age ≥2 yr, wt approximately 10 kg, n = 3). Compound **8b** was formulated in 5% Solutol (neat): 95% PBS at 0.5 mg/mL for IV dosing. This formulation was administered by slow bolus iv injection into the cephalic vein at 0.2 mL/kg (0.1 mg/kg dose; n = 3). Compound **8b** was formulated in 5% Solutol (neat): 95% PBS at 0.25 mg/mL and dosed orally (PO; 2 mL/kg; 0.5 mg/kg; n = 3 animals/compound) by gavage. Blood (approximately 0.3 mL/sample) was collected from the saphenous vein of each animal at 5 min (IV dose only), 15 min, 0.5, 1, 2, 4, 7, and 24 h post-dose. Blood samples were centrifuged at 3000 rpm and the resultant plasma was transferred to a matrix plate and stored frozen until analysis.

PK Sample Preparation and Analysis. Standard curve solutions of each compound were prepared from 10 mg/mL DMSO stock solution diluted into plasma to final concentrations of 1–5000 ng/mL. These standard curve samples were prepared for LC/MS/MS like the PK plasma samples below.

PK plasma samples were thawed and 25 μL aliquots of each sample (or standard curve solution) were transferred to a fresh plate. A 150 μL aliquot of extraction solution (100% acetonitrile containing 100 ng/mL of glyburide as an internal standard) was added to each well. The plate was covered and mixed for approximately 5 min on a pulse-vortex mixer. The plate was centrifuged at 4000 rpm for 10 min at 4 °C. A 125 μL volume of the resulting supernatant was transferred into the corresponding well of a clean 1 mL 96-well assay plate and mixed with 100 μL of water. A 10 μL aliquot of the extract was injected onto an LC/MS/MS system for analysis. HPLC conditions: Agilent 1290, LC column: ACE C18, 30 × 2.0 mm, 3 μm; Acquity C18 50 × 2.1 mm, 3 μm, or equivalent. Flow rate 600–800 μL/min. MS/MS system (*i.e.* ABSciexQ5500, Agilux6500, or similar) and analyzed in the positive mode (each compound was tuned separately from neat methanol stock solution).

PK parameters were derived from plasma concentration values by noncompartmental analysis using Excel. Terminal half-life ($t_{1/2}$) = $-0.693/k_{el}$, where k_{el} is the slope of the line formed from the times of the last 3 measured concentrations *versus* the natural log of the last 3 measured concentrations. Initial concentration (C_0) was set to 0 for PO dosing and to $e^{(\ln(C1)+(\ln(C1)-\ln(C2))/2)}$ for IV dosing. The area under the curve (AUC) was calculated by the linear trapezoidal rule: AUC = $\sum_{i=0}^{n-1} (t_{i+1} - t_i) \times (C_i + C_{i+1})/2$. Extrapolated AUC ($AUC_{ext}$) = AUC + $C_{last} \times t_{1/2}/0.693$, where C_{last} is the last quantifiable concentration. The area under the moment curve (AUMC) was calculated by: AUMC = $\sum_{i=0}^{n-1} (t_{i+1} - t_i) \times (C_i \times t_i + C_{i+1} \times t_{i+1})/2$. Mean residence time (MRT) was calculated by: MRT = AUMC/AUC. Clearance (Cl) was calculated by: CL = (IV Dose)/AUC_{ext}. Volume of distribution (Vd_{ss}) was calculated by: Vd_{ss} = CL × MRT. Bioavailability (% F) was calculated by: % F = 100% × (IV dose × PO AUC)/(PO dose × IV AUC).

■ ASSOCIATED CONTENT

Supporting Information

The Supporting Information is available free of charge at https://pubs.acs.org/doi/10.1021/acs.jmedchem.0c01505.

https://dx.doi.org/10.1021/acs.jmedchem.0c01505
J. Med. Chem. 2021, 64, 2622–2633

Supplemental Table 1, Supplemental Figures S1−S4, and LCMS traces for compounds (PDF)
Molecular formula strings (CSV)

AUTHOR INFORMATION

Corresponding Author

Lauren G. Monovich − *Novartis Institutes for BioMedical Research, Cambridge, Massachusetts 02139, United States;* orcid.org/0000-0001-8455-4171; Email: lauren.monovich@novartis.com

Authors

Andrei A. Golosov − *Novartis Institutes for BioMedical Research, Cambridge, Massachusetts 02139, United States*
Alec N. Flyer − *Novartis Institutes for BioMedical Research, Cambridge, Massachusetts 02139, United States*
Jakal Amin − *Novartis Institutes for BioMedical Research, Cambridge, Massachusetts 02139, United States*
Charles Babu − *Novartis Institutes for BioMedical Research, Cambridge, Massachusetts 02139, United States*
Christian Gampe − *Novartis Institutes for BioMedical Research, Cambridge, Massachusetts 02139, United States*
Jingzhou Li − *Novartis Institutes for BioMedical Research, Cambridge, Massachusetts 02139, United States*
Eugene Liu − *Novartis Institutes for BioMedical Research, Cambridge, Massachusetts 02139, United States*
Katsumasa Nakajima − *Novartis Institutes for BioMedical Research, Cambridge, Massachusetts 02139, United States;* orcid.org/0000-0001-8295-5086
David Nettleton − *Novartis Institutes for BioMedical Research, Cambridge, Massachusetts 02139, United States*
Tajesh J. Patel − *Novartis Institutes for BioMedical Research, Cambridge, Massachusetts 02139, United States*
Patrick C. Reid − *PeptiDream, Inc., Kawasaki, Kanagawa 210-0821, Japan*
Lihua Yang − *Novartis Institutes for BioMedical Research, Cambridge, Massachusetts 02139, United States*

Complete contact information is available at: https://pubs.acs.org/10.1021/acs.jmedchem.0c01505

Author Contributions

A.A.G., A.N.F., and L.G.M. conceptualized the study, wrote the manuscript, and contributed equally; A.A.G. performed the modeling and simulation experiments; A.N.F., C.G., J.L., E.L., K.N., T.J.P., and L.Y. prepared the compounds; J.A. and D.N. performed and analyzed the pharmacokinetic studies; C.B. performed the NMR studies to determine the **1a** solution structure; P.C.R. advised on amino acid selection and technical capabilities of in vitro translation technology. All authors have given approval to the final version of the manuscript.

Author Contributions

[#]A.A.G., A.N.F., and L.G.M. contributed equally to the manuscript.

Notes

The authors declare no competing financial interest.

ACKNOWLEDGMENTS

We acknowledge John Reilly for the column-based profiling data (log D and EPSA); Jennifer Poirier for peptide purification methods; David Ayres, Adey Kefelegn, and Xuena Lin for PAMPA and MDCK-LE data; and Daniel McKay for enabling AMBER parametrization of custom molecules. We also thank Robert Pearlstein, Callum Dickson, and Viktor Hornak for fruitful discussions on the kinetic nature of permeability.

ABBREVIATIONS

AUC, area under the curve; bql, below the limit of quantitation; clog *P*, calculated octanol−water partition coefficient; CsA, Cyclosporine A; CYP3A4, cytochrome P_{450} 3A4; DMSO, dimethylsulfoxide; EPSA, experimental polar surface area; HPLC, high-performance liquid chromatography; IV, intravenous; LCMS, liquid chromatography mass spectrometry; log P_{app}, log of apparent permeability in $cm \cdot s^{-1}$; MDCK-LE, Madin−Darby canine kidney−low efflux cells; MW, molecular weight; nd, not determined; Nle, norleucine; Nle, *N*-methylnorleucine; NMR, nuclear magnetic resonance; PO, per os; PAMPA, parallel artificial membrane permeability assay; Phe, *N*-methylphenylalanine; phe, D-phenylalanine; phe, *N*-methyl-D-phenylalanine; TEA, triethylamine; TFA, trifluoroacetic acid; TIS, triisopropylsilane; TPSA, topological polar surface area

REFERENCES

(1) Vinogradov, A. A.; Yin, Y.; Suga, H. Macrocyclic Peptides as Drug Candidates: Recent Progress and Remaining Challenges. *J. Am. Chem. Soc.* **2019**, *141*, 4167−4181.
(2) Zorzi, A.; Deyle, K.; Heinis, C. Cyclic Peptide Therapeutics: Past, Present and Future. *Curr. Opin. Chem. Biol.* **2017**, *38*, 24−29.
(3) Price, D. A.; Mathiowetz, A. M.; Liras, S. Designing Orally Bioavailable Peptide and Peptoid Macrocycles. In *Practical Medicinal Chemistry with Macrocycles*; Marsault, E., Peterson, M., Eds.; John Wiley & Sons, Inc.: Hoboken, NJ, 2017; pp 59−76.
(4) Rezai, T.; Bock, J. E.; Zhou, M. V.; Kalyanaraman, C.; Lokey, R. S.; Jacobson, M. P. Conformational Flexibility, Internal Hydrogen Bonding, and Passive Membrane Permeability: Successful in Silico Prediction of the Relative Permeabilities of Cyclic Peptides. *J. Am. Chem. Soc.* **2006**, *128*, 14073−14080.
(5) Over, B.; Matsson, P.; Tyrchan, C.; Artursson, P.; Doak, B. C.; Foley, M. A.; Hilgendorf, C.; Johnston, S. E.; Lee, M. D.; Lewis, R. J.; McCarren, P.; Muncipinto, G.; Norinder, U.; Perry, M. W. D.; Duvall, J. R.; Kihlberg, J. Structural and Conformational Determinants of Macrocycle Cell Permeability. *Nat. Chem. Biol.* **2016**, *12*, 1065−1074.
(6) Blanco, M.-J. Building upon Nature's Framework: Overview of Key Strategies Toward Increasing Drug-Like Properties of Natural Product Cyclopeptides and Macrocycles. In *Methods in Molecular Biology*; Goetz, G., Ed.; Humana Press: New York, NY, 2019; Vol. *2001*, pp 203−233.
(7) Foster, A. D.; Ingram, J. D.; Leitch, E. K.; Lennard, K. R.; Osher, E. L.; Tavassoli, A. Methods for the Creation of Cyclic Peptide Libraries for Use in Lead Discovery. *J. Biomol. Screen* **2015**, *20*, 563−576.
(8) Sohrabi, C.; Foster, A.; Tavassoli, A. Methods for Generating and Screening Libraries of Genetically Encoded Cyclic Peptides in Drug Discovery. *Nat. Rev. Chem.* **2020**, *4*, 90−101.
(9) Bozovičar, K.; Bratkovič, T. Evolving a Peptide: Library Platforms and Diversification Strategies. *Int. J. Mol. Sci.* **2020**, *21*, 215−246.
(10) Naylor, M. R.; Bockus, A. T.; Blanco, M.-J.; Lokey, R. S. Cyclic Peptide Natural Products Chart the Frontier of Oral Bioavailability in the Pursuit of Undruggable Targets. *Curr. Opin. Chem. Biol.* **2017**, *38*, 141−147.
(11) Nielsen, D. S.; Shepherd, N. E.; Xu, W.; Lucke, A. J.; Stoermer, M. J.; Fairlie, D. P. Orally Absorbed Cyclic Peptides. *Chem. Rev.* **2017**, *117*, 8094−8128.
(12) Kling, A.; Lukat, P.; Almeida, D. V.; Bauer, A.; Fontaine, E.; Sordello, S.; Zaburannyi, N.; Herrmann, J.; Wenzel, S. C.; König, C.; Ammerman, N. C.; Barrio, M. B.; Borchers, K.; Bordon-Pallier, F.; Brönstrup, M.; Courtemanche, G.; Gerlitz, M.; Geslin, M.; Hammann,

P.; Heinz, D. W.; Hoffmann, H.; Klieber, S.; Kohlmann, M.; Kurz, M.; Lair, C.; Matter, H.; Nuermberger, E.; Tyagi, S.; Fraisse, L.; Grosset, J. H.; Lagrange, S.; Müller, R. Targeting DnaN for Tuberculosis Therapy Using Novel Griselimycins. *Science* **2015**, *348*, 1106−1112.
(13) Nielsen, D. S.; Hoang, H. N.; Lohman, R.-J.; Diness, F.; Fairlie, D. P. Total Synthesis, Structure, and Oral Absorption of a Thiazole Cyclic Peptide, Sanguinamide A. *Org. Lett.* **2012**, *14*, 5720−5723.
(14) Borel, J. F.; Kis, Z. L.; Beveridge, T. The History of the Discovery and Development of Cyclosporine (Sandimmune). In *The Search for Anti-inflammatory Drugs*; Merluzzi, V. J., Adams, J., Eds.; Birkhäuser Boston: Cambridge, MA, 1995; pp 27−63.
(15) Ermert, P.; Luther, A.; Zbinden, P.; Obrecht, D. Frontier Between Cyclic Peptides and Macrocycles. In *Methods in Molecular Biology*; Goetz, G., Ed.; Humana Press: New York, NY, 2019; Vol. *2001*, pp 147−202.
(16) Brayden, D. J.; Hill, T. A.; Fairlie, D. P.; Maher, S.; Mrsny, R. J. Systemic Delivery of Peptides by the Oral Route: Formulation and Medicinal Chemistry Approaches. *Adv. Drug Deliv. Rev.* **2020**, *157*, 2−36.
(17) Boesch, D.; Gavériaux, C.; Jachez, B.; Pourtier-Manzanedo, A.; Bollinger, P.; Loor, F. In Vivo Circumvention of P-Glycoprotein-Mediated Multidrug Resistance of Tumor Cells with SDZ PSC 833. *Cancer Res.* **1991**, *51*, 4226−4233.
(18) Paeshuyse, J.; Kaul, A.; De Clercq, E.; Rosenwirth, B.; Dumont, J.-M.; Scalfaro, P.; Bartenschlager, R.; Neyts, J. The non-immunosuppressive cyclosporin DEBIO-025 is a potent inhibitor of hepatitis C virus replicationin vitro. *Hepatology* **2006**, *43*, 761−770.
(19) Riss, B.; Grandeury, A.; Gut, T.; Seeger-Weibel, M.; Zuercher, C.; Li, J.; Gallou, F. Development of a Practical Process for the Opening of Macrocyclic Cyclosporin A and Amino Acid Deletion. *Org. Process Res. Dev.* **2014**, *18*, 1763−1770.
(20) Tuvia, S.; Atsmon, J.; Teichman, S. L.; Katz, S.; Salama, P.; Pelled, D.; Landau, I.; Karmeli, I.; Bidlingmaier, M.; Strasburger, C. J.; Kleinberg, D. L.; Melmed, S.; Mamluk, R. Oral Octreotide Absorption in Human Subjects: Comparable Pharmacokinetics to Parenteral Octreotide and Effective Growth Hormone Suppression. *J. Clin. Endocrinol. Metab.* **2012**, *97*, 2362−2369.
(21) Hewitt, W. M.; Leung, S. S. F.; Pye, C. R.; Ponkey, A. R.; Bednarek, M.; Jacobson, M. P.; Lokey, R. S. Cell-Permeable Cyclic Peptides from Synthetic Libraries Inspired by Natural Products. *J. Am. Chem. Soc.* **2015**, *137*, 715−721.
(22) Rezai, T.; Yu, B.; Millhauser, G. L.; Jacobson, M. P.; Lokey, R. S. Testing the Conformational Hypothesis of Passive Membrane Permeability Using Synthetic Cyclic Peptide Diastereomers. *J. Am. Chem. Soc.* **2006**, *128*, 2510−2511.
(23) Wang, C. K.; Northfield, S. E.; Colless, B.; Chaousis, S.; Hamernig, I.; Lohman, R.-J.; Nielsen, D. S.; Schroeder, C. I.; Liras, S.; Price, D. A.; Fairlie, D. P.; Craik, D. J. Rational Design and Synthesis of an Orally Bioavailable Peptide Guided by NMR Amide Temperature Coefficients. *Proc. Natl. Acad. Sci. U.S.A.* **2014**, *111*, 17504−17509.
(24) Fouché, M.; Schäfer, M.; Berghausen, J.; Desrayaud, S.; Blatter, M.; Piéchon, P.; Dix, I.; Martin Garcia, A.; Roth, H.-J. Design and Development of a Cyclic Decapeptide Scaffold with Suitable Properties for Bioavailability and Oral Exposure. *ChemMedChem* **2016**, *11*, 1048−1059.
(25) Passioura, T.; Suga, H. Flexizyme-Mediated Genetic Reprogramming as a Tool for Noncanonical Peptide Synthesis and Drug Discovery. *Chem.−Eur. J.* **2013**, *19*, 6530−6536.
(26) Passioura, T.; Suga, H. A RaPID Way to Discover Nonstandard Macrocyclic Peptide Modulators of Drug Targets. *Chem. Commun.* **2017**, *53*, 1931−1940.
(27) Otero-Ramirez, M.; Passioura, T.; Suga, H. Structural Features and Binding Modes of Thioether-Cyclized Peptide Ligands. *Biomedicines* **2018**, *6*, 116−128.
(28) Guillen Schlippe, Y. V.; Hartman, M. C. T.; Josephson, K.; Szostak, J. W. In Vitro Selection of Highly Modified Cyclic Peptides That Act as Tight Binding Inhibitors. *J. Am. Chem. Soc.* **2012**, *134*, 10469−10477.
(29) White, T. R.; Renzelman, C. M.; Rand, A. C.; Rezai, T.; McEwen, C. M.; Gelev, V. M.; Turner, R. A.; Linington, R. G.; Leung, S. S. F.; Kalgutkar, A. S.; Bauman, J. N.; Zhang, Y.; Liras, S.; Price, D. A.; Mathiowetz, A. M.; Jacobson, M. P.; Lokey, R. S. On-Resin N-Methylation of Cyclic Peptides for Discovery of Orally Bioavailable Scaffolds. *Nat. Chem. Biol.* **2011**, *7*, 810−817.
(30) Shinbara, K.; Liu, W.; van Neer, R. H. P.; Katoh, T.; Suga, H. Methodologies for Backbone Macrocyclic Peptide Synthesis Compatible With Screening Technologies. *Front. Chem.* **2020**, *8*, 447.
(31) Leung, S. S. F.; Mijalkovic, J.; Borrelli, K.; Jacobson, M. P. Testing Physical Models of Passive Membrane Permeation. *J. Chem. Inf. Model.* **2012**, *52*, 1621−1636.
(32) Kerns, E. H.; Di, L.; Petusky, S.; Kleintop, T.; Huryn, D.; McConnell, O.; Carter, G. Pharmaceutical Profiling Method for Lipophilicity and Integrity Using Liquid Chromatography-Mass Spectrometry. *J. Chromatogr., B: Anal. Technol. Biomed. Life Sci.* **2003**, *791*, 381−388.
(33) Goetz, G. H.; Philippe, L.; Shapiro, M. J. EPSA: A Novel Supercritical Fluid Chromatography Technique Enabling the Design of Permeable Cyclic Peptides. *ACS Med. Chem. Lett.* **2014**, *5*, 1167−1172.
(34) Peters, S. A. *Physiologically-Based Pharmacokinetic (PBPK) Modeling and Simulations: Principles, Methods, and Applications in the Pharmaceutical Industry*, 1st ed.; John Wiley & Sons, Inc.: Hoboken, New Jersey, 2012.
(35) Rand, A. C.; Leung, S. S. F.; Eng, H.; Rotter, C. J.; Sharma, R.; Kalgutkar, A. S.; Zhang, Y.; Varma, M. V.; Farley, K. A.; Khunte, B.; Limberakis, C.; Price, D. A.; Liras, S.; Mathiowetz, A. M.; Jacobson, M. P.; Lokey, R. S. Optimizing PK Properties of Cyclic Peptides: The Effect of Side Chain Substitutions on Permeability and Clearance. *MedChemComm* **2012**, *3*, 1282−1289.
(36) Furukawa, A.; Townsend, C. E.; Schwochert, J.; Pye, C. R.; Bednarek, M. A.; Lokey, R. S. Passive Membrane Permeability in Cyclic Peptomer Scaffolds Is Robust to Extensive Variation in Side Chain Functionality and Backbone Geometry. *J. Med. Chem.* **2016**, *59*, 9503−9512.
(37) Fouché, M.; Schäfer, M.; Blatter, M.; Berghausen, J.; Desrayaud, S.; Roth, H.-J. Pharmacokinetic Studies around the Mono- and Difunctionalization of a Bioavailable Cyclic Decapeptide Scaffold. *ChemMedChem* **2016**, *11*, 1060−1068.
(38) Lipinski, C. A.; Lombardo, F.; Dominy, B. W.; Feeney, P. J. Experimental and Computational Approaches to Estimate Solubility and Permeability in Drug Discovery and Development Settings. *Adv. Drug Deliv. Rev.* **2012**, *64*, 4−17.
(39) Poongavanam, V.; Danelius, E.; Peintner, S.; Alcaraz, L.; Caron, G.; Cummings, M. D.; Wlodek, S.; Erdelyi, M.; Hawkins, P. C. D.; Ermondi, G.; Kihlberg, J. Conformational Sampling of Macrocyclic Drugs in Different Environments: Can We Find the Relevant Conformations? *ACS Omega* **2018**, *3*, 11742−11757.
(40) Sindhikara, D.; Spronk, S. A.; Day, T.; Borrelli, K.; Cheney, D. L.; Posy, S. L. Improving Accuracy, Diversity, and Speed with Prime Macrocycle Conformational Sampling. *J. Chem. Inf. Model.* **2017**, *57*, 1881−1894.
(41) Dickson, C. J.; Hornak, V.; Pearlstein, R. A.; Duca, J. S. Structure-Kinetic Relationships of Passive Membrane Permeation from Multiscale Modeling. *J. Am. Chem. Soc.* **2017**, *139*, 442−452.
(42) Case, D. A.; Darden, T. A.; Cheatham, T. E., III; Simmerling, C. L.; Wang, J.; Duke, R. E.; Luo, R.; Walker, R. C.; Zhang, W.; Merz, K. M.; Roberts, B.; Hayik, S.; Roitberg, A.; Seabra, G.; Swails, J.; Götz, A. W.; Kolossváry, I.; Wong, K. F.; Paesani, F.; Vanicek, J.; Wolf, R. M.; Liu, J.; Wu, X.; Brozell, S. R.; Steinbrecher, T.; Gohlke, H.; Cai, Q.; Ye, X.; Wang, J.; Hsieh, M.-J.; Cui, G.; Roe, D. R.; Mathews, D. H.; Seetin, M. G.; Salomon-Ferrer, R.; Sagui, C.; Babin, V.; Luchko, T.; Gusarov, S.; Kovalenko, A.; Kollman, P. A. *AMBER 12*; University of California: San Francisco, 2012.
(43) Wang, J.; Cieplak, P.; Kollman, P. A. How Well Does a Restrained Electrostatic Potential (RESP) Model Perform in Calculating Conformational Energies of Organic and Biological Molecules? *J. Comput. Chem.* **2000**, *21*, 1049−1074.

https://dx.doi.org/10.1021/acs.jmedchem.0c01505
J. Med. Chem. 2021, 64, 2622−2633

(44) Bayly, C. I.; McKay, D.; Truchon, J.-F. An Informal AMBER Small Molecule Force Field: parm@Frosst. http://www.ccl.net/cca/data/parm_at_Frosst/parm_Frosst_note.pdf (accessed Nov 1, 2010).
(45) Jakalian, A.; Jack, D. B.; Bayly, C. I. Fast, efficient generation of high-quality atomic charges. AM1-BCC model: II. Parameterization and validation. *J. Comput. Chem.* **2002**, *23*, 1623−1641.
(46) *Schrödinger Release 2012: Protein Preparation Wizard*; Schrödinger, LLC: New York, NY, 2012.
(47) Watts, K. S.; Dalal, P.; Tebben, A. J.; Cheney, D. L.; Shelley, J. C. Macrocycle Conformational Sampling with MacroModel. *J. Chem. Inf. Model.* **2014**, *54*, 2680−2696.
(48) Still, W. C.; Tempczyk, A.; Hawley, R. C.; Hendrickson, T. Semianalytical Treatment of Solvation for Molecular Mechanics and Dynamics. *J. Am. Chem. Soc.* **1990**, *112*, 6127−6129.
(49) Qiu, D.; Shenkin, P. S.; Hollinger, F. P.; Still, W. C. The GB/SA Continuum Model for Solvation. A Fast Analytical Method for the Calculation of Approximate Born Radii. *J. Phys. Chem. A* **1997**, *101*, 3005−3014.
(50) Reddy, M. R.; Erion, M. D.; Agarwal, A.; Viswanadhan, V. N.; McDonald, D. Q.; Still, W. C. Solvation Free Energies Calculated Using the GB/SA model: Sensitivity of Results on Charge Sets, Protocols, and Force Fields. *J. Comput. Chem.* **1998**, *19*, 769−780.
(51) Weiser, J.; Shenkin, P. S.; Still, W. C. Approximate Solvent-Accessible Surface Areas from Tetrahedrally Directed Neighbor Densities. *Biopolymers* **1999**, *50*, 373−380.
(52) Weiser, J.; Shenkin, P. S.; Still, W. C. Approximate Atomic Surfaces from Linear Combinations of Pairwise Overlaps (LCPO). *J. Comput. Chem.* **1999**, *20*, 217−230.
(53) Weiser, J.; Shenkin, P. S.; Still, W. C. Fast, Approximate Algorithm for Detection of Solvent-Inaccessible Atoms. *J. Comput. Chem.* **1999**, *20*, 586−596.
(54) Weiser, J.; Shenkin, P. S.; Still, W. C. Optimization of Gaussian Surface Calculations and Extension to Solvent-Accessible Surface Areas. *J. Comput. Chem.* **1999**, *20*, 688−703.
(55) Banks, J. L.; Beard, H. S.; Cao, Y.; Cho, A. E.; Damm, W.; Farid, R.; Felts, A. K.; Halgren, T. A.; Mainz, D. T.; Maple, J. R.; Murphy, R.; Philipp, D. M.; Repasky, M. P.; Zhang, L. Y.; Berne, B. J.; Friesner, R. A.; Gallicchio, E.; Levy, R. M. Integrated Modeling Program, Applied Chemical Theory (IMPACT). *J. Comput. Chem.* **2005**, *26*, 1752−1780.
(56) Halgren, T. A. MMFF VII. Characterization of MMFF94, MMFF94s, and other widely available force fields for conformational energies and for intermolecular-interaction energies and geometries. *J. Comput. Chem.* **1999**, *20*, 730−748.
(57) Onufriev, A.; Bashford, D.; Case, D. A. Exploring Protein Native States and Large-Scale Conformational Changes with a Modified Generalized Born Model. *Proteins* **2004**, *55*, 383−394.
(58) Guzaev, A.; Manoharan, M. Conjugation of Oligonucleotides via an Electrophilic Tether: N-Chloroacetamidohexyl Phosphoramidite Reagent. *Bioorg. Med. Chem. Lett.* **1998**, *8*, 3671−3676.
(59) Goetz, G. H.; Farrell, W.; Shalaeva, M.; Sciabola, S.; Anderson, D.; Yan, J.; Philippe, L.; Shapiro, M. J. High Throughput Method for the Indirect Detection of Intramolecular Hydrogen Bonding. *J. Med. Chem.* **2014**, *57*, 2920−2929.
(60) Dickson, C. J.; Hornak, V.; Bednarczyk, D.; Duca, J. S. Using Membrane Partitioning Simulations to Predict Permeability of Forty-Nine Drug-Like Molecules. *J. Chem. Inf. Model.* **2019**, *59*, 236−244.
(61) Zhou, L.; Yang, L.; Tilton, S.; Wang, J. Development of a high throughput equilibrium solubility assay using miniaturized shake-flask method in early drug discovery. *J. Pharm. Sci.* **2007**, *96*, 3052−3071.

https://dx.doi.org/10.1021/acs.jmedchem.0c01505
J. Med. Chem. 2021, 64, 2622−2633